




# Green synthesis of GO-loaded Ag/ZnO nanocomposites for methyl orange degradation

Digambar Y. Nadargi<sup>1,2,\*</sup> , Jyoti D. Nadargi<sup>3</sup>, Mohaseen S. Tamboli<sup>4</sup>, Asiya M. Tamboli<sup>4</sup>, Imitaz S. Mulla<sup>5</sup>, Ahmad Umar<sup>6</sup>, Nguyen Tam Nguyen Truong<sup>7,\*</sup>, and Sharad S. Suryavanshi<sup>1,\*</sup>

<sup>1</sup> School of Physical Sciences, Punyashlok Ahilyadevi Holkar Solapur University, Solapur, India

<sup>2</sup> Centre for Materials for Electronics Technology, (C-MET), Thrissur, India

<sup>3</sup> Department of Physics, Santosh Bhimrao Patil College, Mandrup, Solapur, India

<sup>4</sup> Korea Institute of Energy Technology (KENTECH), Naju-Si, Jeollanam-do, Republic of Korea

<sup>5</sup> Former Emeritus Scientist, NCL, Pune, India

<sup>6</sup> Department of Chemistry, Najran University, Najran, Kingdom of Saudi Arabia

<sup>7</sup> School of Chemical Engineering, Yeungnam University, Gyeongsan, Republic of Korea

Received: 29 March 2023

Accepted: 10 July 2023

Published online:

22 July 2023

© The Author(s), under exclusive licence to Springer Science+Business Media, LLC, part of Springer Nature 2023

## ABSTRACT

Nature is a perfect laboratory for creating novel nanomaterials for a variety of applications. A robust green synthesis approach to GO-loaded Ag/ZnO nanocomposite materials using medicinal plant extraction and their potential application in methyl orange dye degradation are reported. The straightforward technique employs zinc and silver nitrate precursors in an aqueous solution of medicinal plant extract, causing the precipitation process. Prior to photocatalytic investigations, the physico-chemical properties of the material are analysed using TG-DTA, XRD, FE-SEM, TEM, EDAX and BET. The developed material showcase hexagonal wurtzite structure of ZnO, with face-centered-cubic phase of Ag and AgCl. All the samples exhibit aggregated, irregular rounded grains, as expected in the precipitation synthesis process. Pristine ZnO showed 15.5% degradation efficiency towards methyl orange, which was further improved by doping Ag from 0.5 to 2 mol%. The catalyst with 1 mol% Ag doping resulted in the better photocatalytic activity (26.30%), which has again improved by loading the GO (27.46%). The outcome of this study provides the new insights to GO-loaded Ag/ZnO nanocomposites by green synthesis route, in view of photocatalytic applications.

Address correspondence to E-mail: digambar\_nadargi@yahoo.co.in; tamnguyentn@ynu.ac.kr; sssuryavanshi@rediffmail.com

<https://doi.org/10.1007/s10854-023-10979-6>

## 1 Introduction

Nature is an absolute laboratory, providing inspiration and avenues for the creation of innovative nanomaterials for a wide range of applications. It has varieties of simple recipes to obtain complex materials, structures, dimensions, and many more. Given the rising carbon footprint and environmental pollution, green synthesis routes are more beneficial for resolving environmental toxicity concerns. It is in our best interest to use these cost-effective, non-harmful techniques in the long term. With this motivation, the present efforts demonstrate the straightforward route of developing metal oxide (particularly ZnO) nanoparticles for dye degradation (methyl orange in the present case) under Uv-Visible irradiation.

Speaking about Zinc oxide (ZnO), it has numerous applications in medicine, cosmetics, bio and gas sensors, photocatalysis, drug delivery and many more, due to its fascinating properties such as low toxicity, antimicrobial, biodegradability and cost-effectiveness [1–4]. To date, various synthesis routes have been employed for the development of ZnO nanoparticles, viz. sol-gel method, mechanical milling, spray pyrolysis, organometallic synthesis, thermal evaporation and hydro/solvothermal techniques [5–10]. However, all these approaches use organic solvents and toxic reducing agents, which are extremely reactive and unfriendly to the environment. Green synthesis approaches come to mind as a solution to these problems due to their aforementioned properties (cost-effective, non-harmful and environmental friendly techniques). Amongst the different green routes, plant extract is one of the simple and promising strategy for nanomaterials synthesis [2]. Their extracts can be extracted from the plants, flowers, leaves, fruits, roots, and stems. Plant extracts contain biomolecules and secondary metabolites such as flavanones, tannins, polyphenols, alkaloids, saponins, and terpenoids, which serve as effective reducing agents of zinc precursor [11–13]. Figure 1 depicts a green route method for creating different metal oxide nanoparticles utilizing micro-organisms, seeds, and other natural resources.

ZnO is a popular photocatalyst for environmental remediation because of its low cost, large surface area, excellent electrochemical stability and high electron mobility [14–17]. However, its photocatalytic

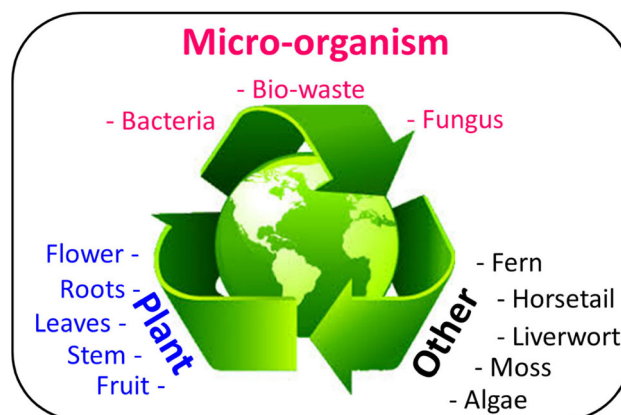


**Fig. 1** Schematic illustration of possible green chemistry through various means

efficiency lags behind due to rapid recombination of photo-excited holes and electrons. The properties of these semiconductors can be modified by adding noble metals and their halides because of their admirable catalytic activity [18–20]. Amongst the various metal halides, Ag/AgCl the most attractive material due to its high chemical stability and electrical conductivity [21–23]. Visible-light photodegradation, water photolysis, photoelectric detection, and bacterial disinfection are all common applications for Ag/AgCl [24, 25]. The photocatalyst Ag/AgCl is based on the effects of nanometal surface plasmon resonance (SPR) and semiconductor photocatalysis. The SPR effect generates and separates electrons and holes. Because of surface electron oscillation, electron-hole pairs are formed in nanosilver when exposed to visible light. Considering the polarisation of the electric field, electrons are then transferred to the surface of the Ag nanoparticles to create reactive oxygen groups. The holes are transported to the AgCl contact, where Cl ions are oxidised to Cl atoms. These Cl atoms can then oxidise organic dyes to produce Cl ions once again. Ag nanoparticles absorb photons. Photoelectrons are trapped in Ag nanoparticles and are not transported to silver ions. Throughout this process, AgCl is not consumed and thus is a stable photocatalyst [26].

However, restricted control of doping process in general (which is  $\sim 10\%$ ) needs another approach in the enhancement of visible light absorption of ZnO. It can be overcome by combining semiconductor materials with mesoporous materials. In accordance with this, carbonaceous materials such as graphene can be a suitable candidate due to its electronic

properties, unique pore structure and larger surface area [27, 28].

In the present study, we are going to show the simple, cost-effective, non-toxic and greener synthesis approach using medicinal plant extract for synthesis of GO-loaded Ag/ZnO nanocomposites and their potential use in the methyl orange dye degradation under Uv-Vis irradiated photocatalysis. The addition of GO is intended to increase the surface area. Both the large surface area and the high porosity are advantageous for enhancing the photocatalytic activity of the produced samples.

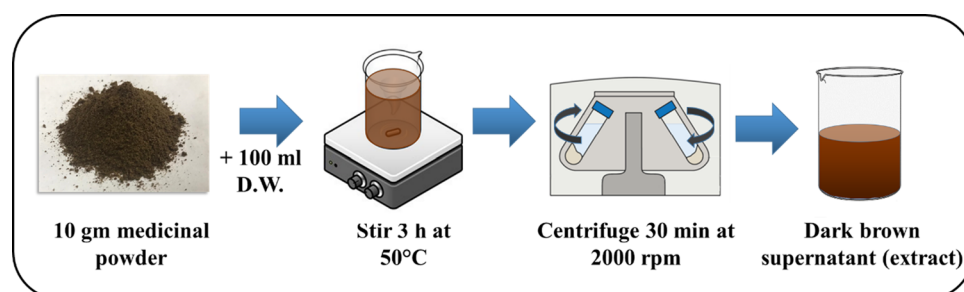
## 2 Experimental

The chemicals used in the typical synthesis are: zinc nitrate hexahydrate ( $\text{Zn}(\text{NO}_3)_2 \cdot 6\text{H}_2\text{O}$  purum grade, graphene oxide (GO), and silver nitrate ( $\text{AgNO}_3$ ) trace metal basis; all obtained from Sigma-Aldrich. The required plant-powder for green synthesis was obtained from proprietary brand of medicinal powders (Patanjali, India) through local supplier. The details of plant-powder (ingredients with their wt%) are detailed in the supplementary section (ESI-1, Table—S1). The extract preparation and the entire synthesis process were carried out using double distilled water (DW).

### 2.1 Extract preparation

For the extract preparation, 10 g of plant-powder was dissolved in 100 mL of distilled water. At 50 °C the mixture was stirred for 3 h and then allowed to cool down to the room temperature. After centrifuging the mixture at 2000 rpm for 30 min, the extract was collected in a different beaker and kept separate for green synthesis. Fig. 2, shows the schematic of extract synthesis process.

**Fig. 2** Schematic of medicinal powder extract synthesis

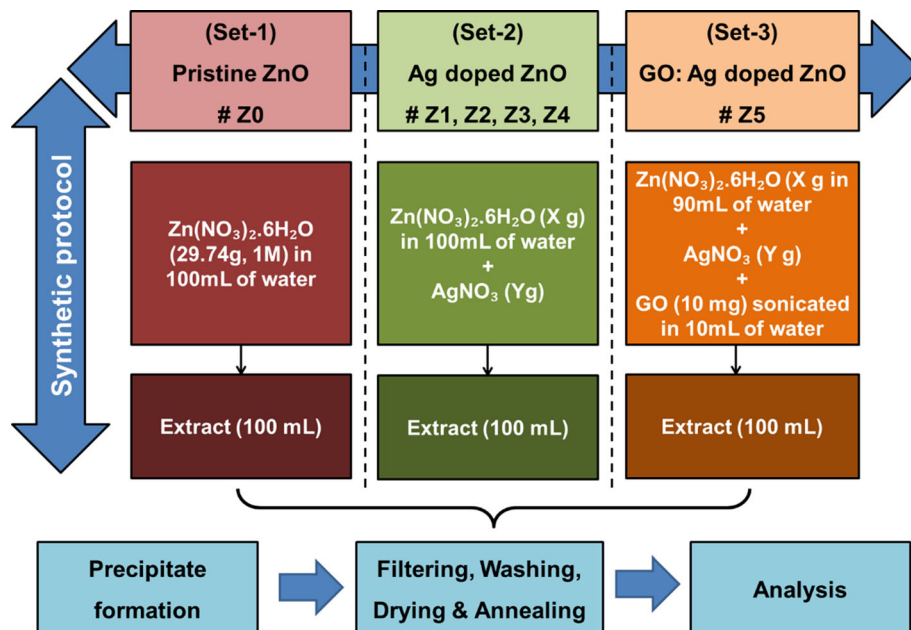


### 2.2 Preparation of pristine ZnO, Ag/ZnO, and GO-Ag/ZnO

Fig. 3 showcase the synthetic protocol of three sample sets: (i) pristine ZnO, (ii) Ag/ZnO, and (iii) GO-Ag/ZnO.

Pure ZnO nanoparticles (Set-1) were prepared by dissolving  $\text{Zn}(\text{NO}_3)_2 \cdot 6\text{H}_2\text{O}$  (29.74 g, 1 M) in 100 mL DW and then slowly and dropwise addition of extract (100 mL) in a volume equivalence was done. This method of extract addition is favored because rapid addition results into an inhomogeneous reaction mixture, resulting in the formation of larger particles. The Set-2 of having Ag/ZnO nanoparticles was synthesized as of pristine ZnO, simply by replacing a mol fraction of zinc nitrate with equivalent mol fraction of silver nitrate. The variation of mol fraction was made from 0.5 to 2.0 mol% with the step of 0.5. Finally, nanoparticles of GO-Ag/ZnO (Set-3), were prepared by adding 10 mg of GO to the reacting mixture of the optimized Ag/ZnO sample (1 mol% doped Ag in ZnO) from Set-2. In order to disperse the GO properly in the reaction medium, GO was ultrasonicated for 15 min in 10 mL DW before the addition of extract in the precursor solution. This 10 mL sonicated GO solution was added to 90 mL of precursor solution to balance/equalise the concentration of the reaction mixture in each set. Finally, as obtained precipitates of ZnO from all the sample sets, were filtered, washed, dried and annealed at 400 °C for 2 h in air, respectively. The annealed samples were labelled as Z0 to Z5 starting from Set-1 to Set-3, with Z0 = pristine ZnO, Z1–Z4 = 0.5–2.0 mol% Ag-doped ZnO, and Z5 = GO/Ag (1 mol%) doped ZnO, respectively. The details of material characterizations and photocatalytic study are given in the supplementary section (ESI-2).

**Fig. 3** Schematic of synthesis protocol of three sample sets: (i) pristine ZnO, (ii) Ag/ZnO and (iii) GO-Ag/ZnO



### 3 Results and discussion

#### 3.1 Thermogravimetric analysis (TGA-DTA)

Figure 4 illustrates the TG-DTA plot of sample Z0 and Z2 which shows the three similar distinct weight losses at: (i)  $\sim 29.05\%$  from room temperature to  $150.85^\circ\text{C}$ , (ii)  $\sim 30.08\%$  from  $150.85$  to  $380.68^\circ\text{C}$  and (iii)  $\sim 19.01\%$  from  $380.68$  to  $418^\circ\text{C}$ . The first weight loss in the observed TGA and endothermic peak corresponding  $\sim 100^\circ\text{C}$  in DTA is associated with the decomposition of chemisorbed water molecules. The proper oxide phase formation is completed at  $400^\circ\text{C}$  from where no considerable weight loss is detected. Therefore, all the samples under investigation were calcined at  $400^\circ\text{C}$ .

#### 3.2 Crystallographic and elemental analyses (XRD and EDX)

The X-ray diffraction patterns of pure ZnO, 1 mol% Ag-doped ZnO and GO-Ag-doped ZnO are displayed in Fig. 5. All the diffraction peaks of pure ZnO (Sample Z0) are matching with hexagonal wurtzite structure of ZnO (JCPDS card no. 36-1451, highlighted in red). The major peaks at  $2\theta = 31.82^\circ, 34.52^\circ, 36.36^\circ, 45.54^\circ, 56.70^\circ, 62.96^\circ, 66.46^\circ, 68.04^\circ$  and  $69.16^\circ$  correspond to the (1 0 0), (0 0 2), (1 0 1), (1 0 2), (1 1 0), (1 0 3), (2 0 0), (1 1 2) and (2 0 1) lattice planes of hexagonal wurtzite ZnO, respectively. The XRD

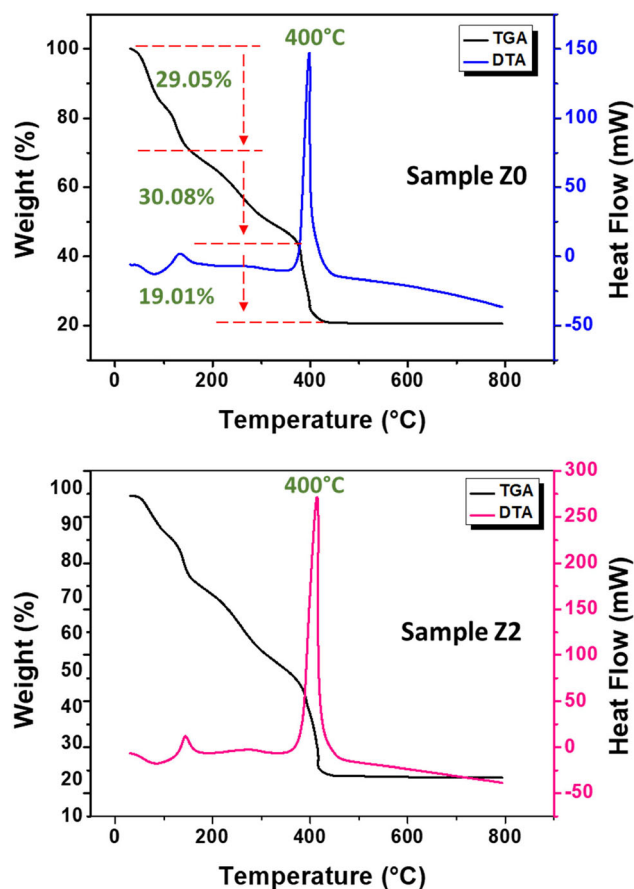


**Fig. 4** TG-DTA plot of sample Z0 and Z2

graphs showed the formation of highly oriented peak along (1 0 0) (0 0 2) and (1 0 1) plane indicating highly

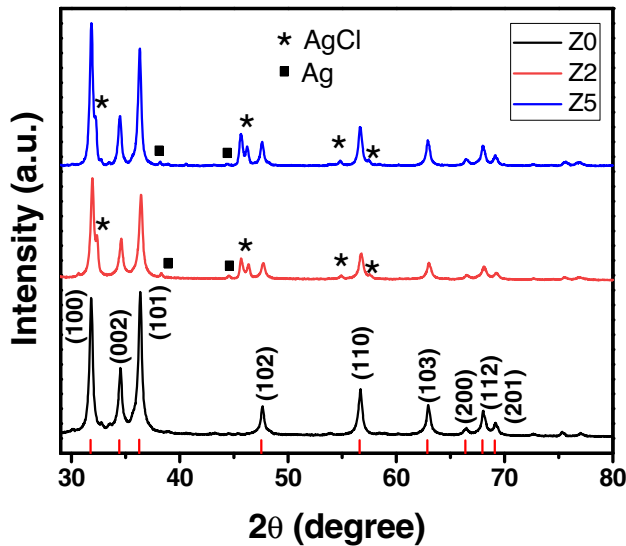


**Fig. 5** XRD patterns of the pristine ZnO along with Ag/ZnO and GO/Ag/ZnO

crystalline material. The crystallites size of 53 nm was determined using FWHM for most intense peak (1 0 1) using Scherrer formula [29].

$$D = \frac{K\lambda}{\beta \cos \theta}, \tag{1}$$

where ‘λ’ is the wavelength of X-ray radiation used, ‘β’ is FWHM (in radians), ‘θ’ the angle of refraction, and ‘K’ is the Scherrer constant. K in the Scherrer equation is not known for the present material system. K can have values anywhere from 0.62 and 2.08. In this paper, K = 0.98 was used. Therefore, all D calculations are only estimates.

The stacked XRD spectra of optimized Ag-doped ZnO sample (Z2) and GO-loaded Ag-doped ZnO sample (Z5) showed the additional characteristic diffraction peaks at  $2\theta = 38.16^\circ$  and  $44.36^\circ$  which are ascribed to the face-centered-cubic phase of metallic Ag (JCPDS No. 04-0783), while at  $2\theta = 32.14^\circ, 45.62^\circ, 46.22^\circ, 54.82^\circ$  and  $57.52^\circ$  are ascribed to the characteristic diffraction peaks of cubic AgCl (JCPDS 00-006-0480). The Ag peaks are not so prominent and hard to find due to low content of Ag doping in the ZnO matrix. There is no shift in the peaks of ZnO after Ag doping; however, slight peak broadening is observed, indicating the possibility of Ag going into the lattice of ZnO [30].

Moreover, the EDX analysis of pristine ZnO (Fig. 6a) and optimized Ag-doped ZnO sample-Z2 (Fig. 6b) revalidated the presence of Zn, O, Ag, and Cl elements in their respective amounts.

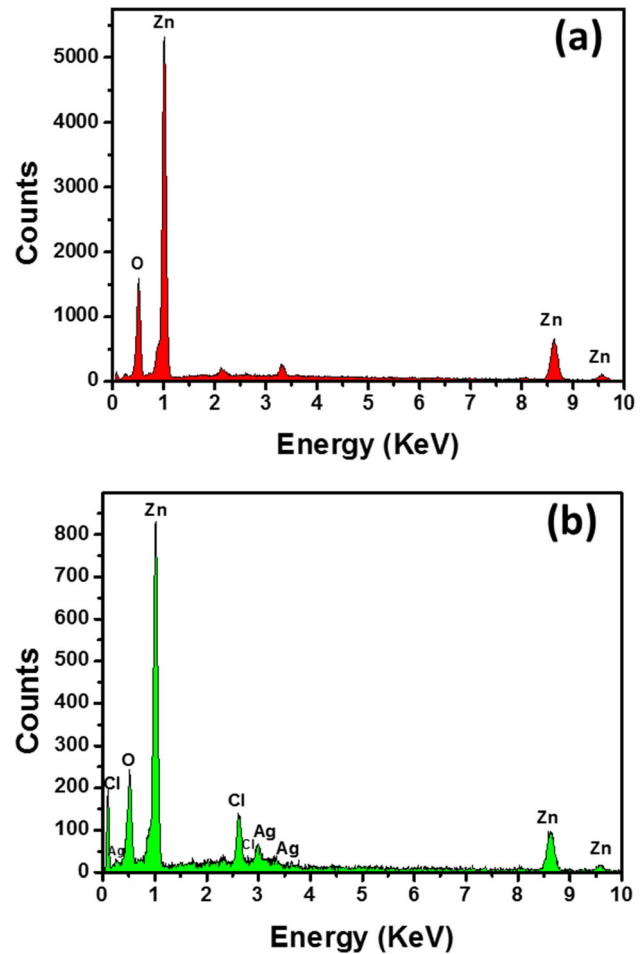


**Fig. 6** EDX patterns of a pristine ZnO along with b 1.0 mol% Ag-doped ZnO

### 3.3 Morphological analysis (SEM and TEM):

The surface morphology of as developed samples was studied using SEM and TEM analyses. The SEM and TEM images (Figs. 7 and 8) of various compositions of Ag/ZnO along with GO loading, confirmed the co-existence of Ag and GO in the ZnO matrix. Figure 7 shows the SEM images of pristine ZnO along with Ag-doped ZnO and GO-loaded Ag-doped ZnO samples. All the samples exhibits aggregated, irregular rounded grains, as expected in the precipitation synthesis process. In Fig. 7, Z5 confirms the agglomerated cluster of graphene oxide along with Ag/ZnO nanoparticles. The micrographs clearly explains the number of empty spaces which facilitate the easy absorption of dye solution during the photocatalytic process thereby its improved kinetics.

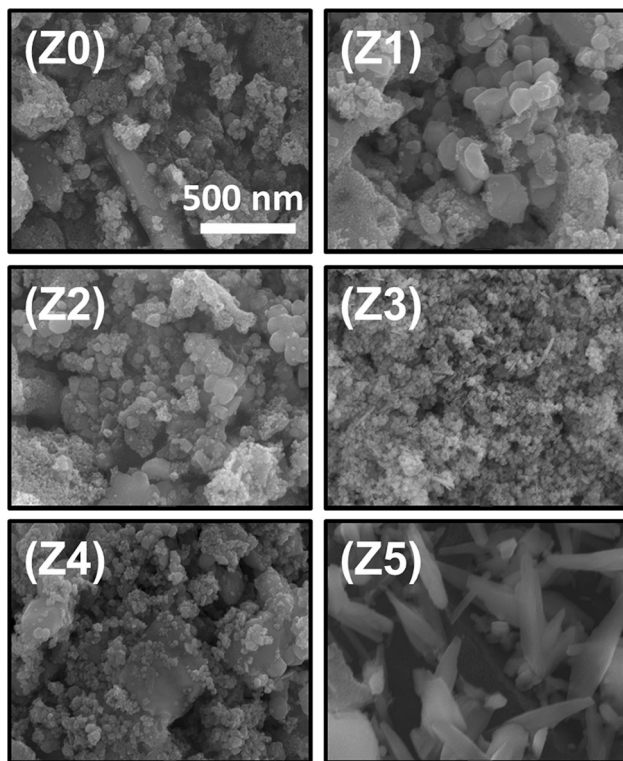


**Fig. 7** SEM images of all the developed samples Z0-Z5, respectively

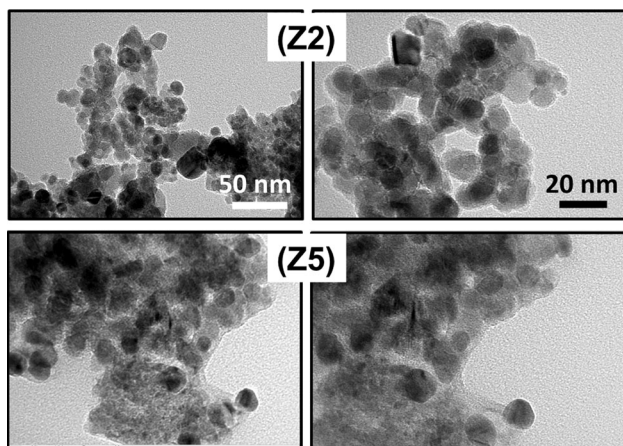


**Fig. 8** TEM images of sample Ag/ZnO (Z2) and GO/Ag/ZnO (Z5)

Further, SEM analysis demonstrates that ZnO has a porous structure (thereby, expecting low density), which is advantageous for photocatalytic applications. At low concentration of Ag doping (sample Z1), it was observed that Ag NPs have a very small dimension, and hence barely change in the morphology of pristine ZnO matrix. However, as the concentration of Ag (Sample Z2–Z5) was increased, a

large number of Ag aggregates appeared on the surface of dispersed and porous ZnO structures. This is likely due to the effect of Ag doping on the crystallization and proliferation of ZnO nanoparticles during precipitation process and thereby calcination.

To further validate the existence of Ag NPs and GO, TEM analysis (Fig. 8) was performed on the with the highest photocatalytic activity (samples Z2 and Z5). On the surface of ZnO, Ag nanoparticles can be seen to be firmly anchored and uniformly distributed. It revalidated the formation of irregular rounded particles observed through SEM analysis. It is observed that Ag nanoparticles doped into ZnO nanoparticles are of 10–12 nm in diameter size. Furthermore, TEM of sample Z5 (Graphene-Ag/ZnO) shows the spherical shaped Ag and ZnO nanoparticles that are randomly distributed and spread-over on the surface of graphene layer.

### 3.4 Surface area analysis (BET)

The  $N_2$  sorption studies shown in Fig. 9 displays a typical IV isothermic activity with a well described hysteresis loop of type H3 (indication of the rounded particles) at  $p/p_0 > 0.8$ , which are obtained in pristine ZnO, Ag-ZnO and GO/Ag-ZnO isotherms. The developed samples showcase the typical mesopore structure. The existence of mesopores is indicated by a significant rise in the adsorbate volume of type IV in the low  $p/p_0$  region. As the deterioration of the adsorbing mass ( $p/p_0 = 0.2$  to 0.8) is normally related to capillary condensation in mesoporous structures,

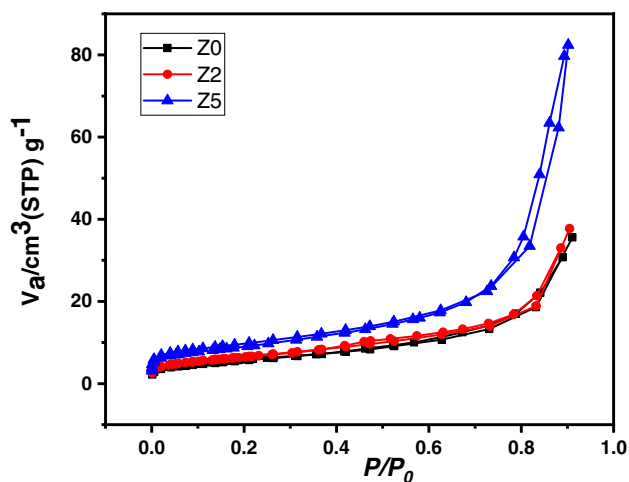


**Fig. 9** BET isotherm curves of ZnO, Ag-doped ZnO and Graphene-Ag/ZnO

capillary condensation is induced below the predicted condensing intensity. It is a secondary mechanism that involves the pre-formation in the pore-walls of multi-layer adsorption of the adsorbed layer. In this case, the two processes in the given area seem to occur concurrently resulting in fewer adsorbed space.

Table 1 tabulates the results of average pore radius, pore volume, and surface area of all the samples. The surface area and pore size analyses of the ZnO nanocomposites revalidates the mesoporous framework of GO/Ag/ZnO with considerable increase in the surface area upon loading GO in the optimised Ag/ZnO sample. The obtained large surface area and high porosity are favorable to enhance the photocatalytic activity of the obtained samples.

### 3.5 Photocatalytic properties

The photocatalytic properties of the developed samples were studied for methyl orange dye degradation under the irradiation of UV light. A sample of 100 mg of catalysts were considered for the degradation of 20 ppm aqueous methyl orange (MO) solution on illumination with 365 nm Hg vapor lamp. The absorption spectra of MO solution and other decomposed solution have been taken over a regular interval of 30 min for 210 min. The degradation parameters are tabulated in Table 2.

The developed ZnO and its derivatives synthesized by green route chemistry shows the decent photocatalytic activity (Fig. 10a–c). There is a decent MO degradation within 210 min by all the catalysts, with a blue shift in the absorption peak.

It can be seen that the photocatalytic activity towards degradation of methyl orange has improved from pristine ZnO to Ag/ZnO to GO-Ag/ZnO samples. Pristine ZnO showed 15.5% degradation efficiency, whereas Ag/ZnO and GO-Ag/ZnO have shown 26.30% and 27.46% degradation efficiency towards methyl orange. An improvement in the degradation property of GO-Ag/ZnO catalyst is mainly due to graphene oxide which has not only

**Table 2** Details of photocatalysis dye degradation parameters

1	Dye	Methyl orange
2	Concentration	20 ppm
3	Photocatalyst amount	100 mg/100 mL
4	Degradation time	210 min
5	Degradation efficiency	25.3
6	pH	7
6	Source of light	365 nm Hg Vapor lamp

facilitated the number of active sites, but also acted as an electron-acceptor/transport for the migration of photo generated electrons and thereby hinders the electron–hole recombination [31]. Moreover, surface area plays a crucial role in enhancing photocatalytic performance. As seen in the BET, GO-Ag/ZnO sample showed highest surface area of 33.99 m<sup>2</sup>/g. The results obtained for the photocatalytic activity of the ZnO, Ag/ZnO and GO-Ag/ZnO are in good agreement with those obtained by BET surface area (Fig. 9).

Table 3 shows the % degradation of methyl orange, during course of irradiation time.

### 3.6 Mechanism of photocatalytic degradation of methyl orange by GO/Ag/ZnO

In general, the photocatalytic degradation of dye by a semiconductor catalyst upon Uv/Vis light irradiation mainly involves two mechanisms: i) excitation of semiconductor and ii) excitation of organic dye. In the first case, an excitation of metal oxide results in the formation of electron/hole pair generation (electrons in the conduction band and holes in the valence band). The as-generated charges drag the organic moieties/pollutants to undergo chemical reactions. In the latter case, an excitation of organic dye leads to transfer of electrons towards electron acceptors to form a cationic dye radical followed by self-degradation or degradation by the reactive oxidation species.

**Table 1** Mean pore radius, pore volume and BET surface area of as developed ZnO nanocomposites

Sample id	Avg. pore radius (nm)	Pore volume (cm <sup>3</sup> /g)	Surface area (m <sup>2</sup> /g)
Z0	10	0.05	19.82
Z2	11	0.05	23.31
Z5	15	0.12	33.99

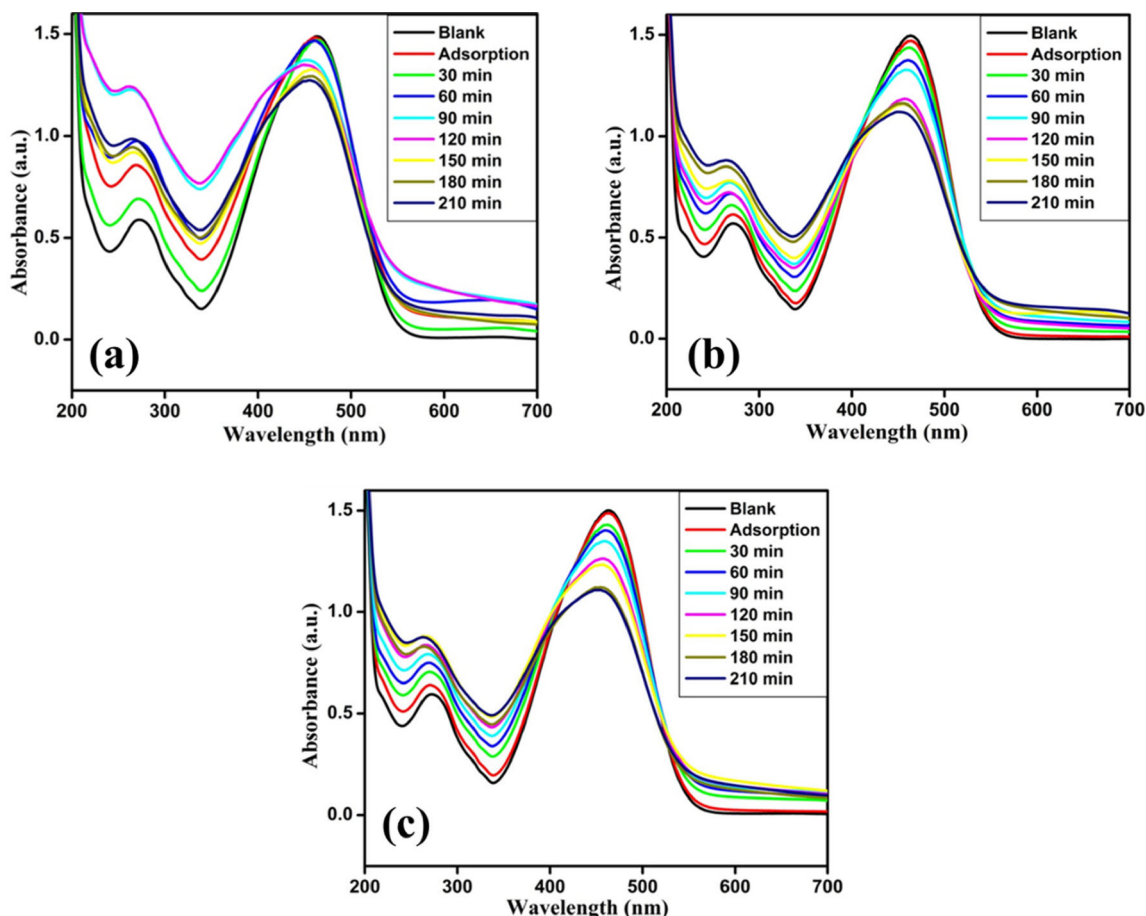


**Fig. 10** a–c Photocatalytic dye degradation of a ZnO, b 1 mol% Ag/ZnO, and c GO-1 mol% Ag/ZnO with 30 min time interval

**Table 3** Percent degradation of methyl orange dye for the samples Z0, Z2, and Z5, respectively

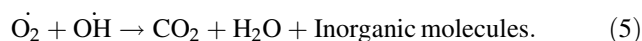
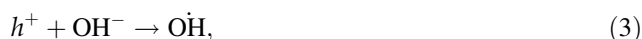
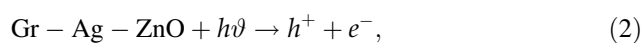
S. no	Sample Z0: Pristine ZnO	Sample Z2: 1 mol% Ag/ZnO	Sample Z5: GO-1 mol% Ag/ZnO
Time	% Degradation of MB	% Degradation of MB	% Degradation of MB
Blank	0.00	0.00	0.00
Adsorption	0.60	1.74	1.00
30 min	1.20	3.86	4.75
60 min	1.70	8.23	6.75
90 min	9.10	11.50	10.44
120 min	11.05	21.45	16.40
150 min	11.55	23.18	18.60
180 min	14.00	23.26	26.30
210 min	15.50	26.30	27.46

In the present Graphene-Ag/ZnO nanocomposites, ZnO undergoes excitation, which means electrons present in the valence band can be excited to the conduction band resulting in hole formation in the valence band due to wide band gap of Ag/ZnO. The excited electrons can be transferred to graphene,

silver nanoparticles and methyl orange dye. Finally, the generated electrons react with dissolved oxygen molecules in the form of oxygen peroxide radicals. The reaction between photogenerated holes and the hydroxide ion derived from water can produce hydroxyl radicals. Degradation of methyl orange



under UV-light can also be due to excitation of dye itself forming electrons/hole pairs. These excited electrons can be transferred from the excited dye to the conduction band of ZnO that undergoes the formation of reactive oxidation species. Thus, a methyl orange dye gets decomposed [32–34]. Fig. 11 shows the schematic illustration of photo-dye degradation using ZnO/Ag–AgCl catalyst.



## 4 Conclusions

In conclusion, this article presents the results of the preparation of pure ZnO, Ag/ZnO and GO-Ag/ZnO nanocomposites through a facile green synthesis approach using medicinal powder extract. The physico-chemical analyses by XRD, SEM, TEM, BET, EDAX revealed the important structural, morphological, and elemental properties of the developed nanoparticles. In the application part, the developed material has proved its potentiality in photocatalytic dye degradation of methyl orange. The photocatalytic activity towards degradation of MO has improved from pristine ZnO to Ag/ZnO to GO-Ag/ZnO samples, as 15.50 to 26.30 to 27.46% degradation efficiency, respectively. The improvement in the photocatalytic activity is due to an enhancement in the surface area (validated by BET), and narrowing

down the wide band gap of ZnO by Ag/AgCl and graphene oxide layer. This has certainly minimized the recombination of photo-induced electrons, resulting in the more amount of methyl orange decomposition. The developed route shows the new insights of green route synthesis of GO-loaded Ag/ZnO nanocomposites for photocatalytic applications.

## Acknowledgements

The authors greatly acknowledge the CSIR, India, for financial support of this work (03(1389)/16/EMR-II).

## Author contributions

Writing-original draft, and Investigation: DN, JDN. Methodology: MST, AMT. Validation: AU, NTNT. Conceptualization: IM, SSS.

## Funding

Dr. Nadargi acknowledges the CSIR, India, for awarding Research Associate under the same scheme.

## Data availability

Data available on request.

## Declarations

**Conflict of interest** The authors declare no competing interests.

**Consent for publication** Not applicable.

**Supplementary Information:** The online version contains supplementary material available at <http://doi.org/10.1007/s10854-023-10979-6>.

## References

1. X. Chen, Z. Wu, D. Liu, Z. Gao, *Nanoscale Res. Lett.* **12**, 143–153 (2017)
2. D.Y. Nadargi, R.B. Dateer, M.S. Tamboli, I.S. Mulla, S.S. Suryavanshi, *RSC Adv.* **9**(58), 33602–33606 (2019)

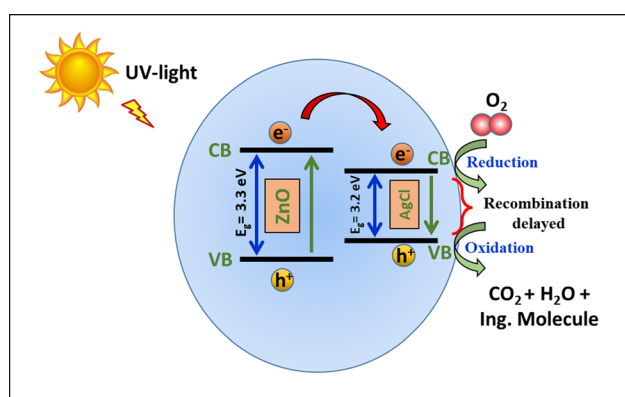


**Fig. 11** Schematic illustration of photo-dye degradation using ZnO/Ag–AgCl catalyst

3. A.F. Shaikh, S.S. Arbuj, M.S. Tamboli, S.D. Naik, S.B. Rane, B.B. Kale, *Chem. Select.* **2**(28), 9174–9180 (2017)
4. M. Khatami, H.Q. Alijani, H. Heli, I. Sharifi, *Ceram. Int.* **44**(13), 15596–15602 (2018)
5. M.F. Khan, A.H. Ansari, M. Hameedullah, E. Ahmad, F.M. Husain, Q. Zia, U.M.R. Baig, M.M. Alam, A.M. Khan, Z.A. Al-Othman, *Sci. Rep.* **6**(1), 1–2 (2016)
6. L.C. Damonte, L.M. Zélis, B.M. Soucase, M.H. Fenollosa, *Chem. Select.* **148**(1), 15–19 (2004)
7. J.K. Saha, R.N. Bukke, N.N. Mude, J. Jang, *Sci. Rep.* **10**(1), 1–1 (2020)
8. K.L. Orchard, M.S. Shaffer, C.K. Williams, *Chem. Mater.* **24**(13), 2443–2448 (2012)
9. B. Abdallah, M. Kakhia, A. Obaide, *Plasmonics* **16**, 1549–1556 (2021)
10. A. Moulahi, F. Sediri, *Optik* **127**(19), 7586–7593 (2016)
11. J. Irvanli, *Green Chem.* **13**(10), 2638–2650 (2011)
12. A.K. Mittal, Y. Chisti, U.C. Banerjee, *Biotechnol. Adv.* **31**(2), 346–356 (2013)
13. S. Ahmed, S.A. Chaudhry, S. Ikram, *J. Photochem. Photobiol. B.* **166**, 272–284 (2017)
14. S.S. Wagh, V.S. Kadam, C.V. Jagtap, D.B. Salunkhe, R.S. Patil, H.M. Pathan, S.P. Patole, *ACS Omega* **8**(8), 7779–7790 (2023)
15. S. Sarkar, D. Basak, *Cryst. Eng. Commun.* **15**(37), 7606–7614 (2013)
16. R.C. Pawar, D. Cho, C.S. Lee, *Curr. Appl Phys.* **5**(13)(2), S50–S57 (2013)
17. R.C. Pawar, H. Kim, C.S. Lee, *Scr. Mater.* **68**(2), 142–145 (2013)
18. X.L. Yu, J.G. Song, Y.S. Fu, Y. Xie, X. Song, J. Sun, X.W. Du, *J. Phys. Chem. C.* **114**(5), 2380–2384 (2010)
19. Z. Guo, X. Chen, J. Li, J.H. Liu, X.J. Langmuir, *Chem. Select.* **27**(10), 6193–6200 (2011)
20. O. Lupan, L. Chow, L.K. Ono, B.R. Cuenya, G. Chai, H. Khallaf, S. Park, A. Schulte, *J. Phys. Chem. C.* **114**(29), 12401–12408 (2010)
21. Y. Zheng, L. Zheng, Y. Zhan, X. Lin, Q. Zheng, K. Wei, *Inorg. Chem.* **46**(17), 6980–6986 (2007)
22. X.Z. Li, F.B. Li, *Environ. Sci. Technol.* **35**(11), 2381–2387 (2001)
23. M.J. Height, S.E. Pratsinis, O. Mekasuwandumrong, P. Praserthdam, *Appl. Catal. B.* **63**(3–4), 305–312 (2006)
24. X. Wang, X. Liu, Q. Han, P. Guo, J. Zhu, R. Yin, *Inorg. Chem. Commun.* **112**, 107716 (2020)
25. S. Gunal, N. Kaloglu, I. Ozdemir, S. Demir, I. Ozdemir, *Inorg. Chem. Commun.* **21**, 142 (2012)
26. S. Tao, M. Yang, H. Chen, S. Zhao, G. Chen, *Ind. Eng. Chem. Res.* **57**(9), 3263 (2018)
27. K. Saoud, R. Alsoubaihi, N. Bensalah, T. Bora, M. Bertino, J. Dutta, *Mater. Res. Bull.* **63**, 134–140 (2015)
28. N.A. Al-Rawashdeh, O. Allabadi, M.T. Aljarrah, *ACS Omega* **5**(43), 28046–28055 (2020)
29. P. Scherrer, *Nachr. Ges. Wiss. Göttingen* **26**, 98–100 (1918)
30. S.S. Wagh, C.V. Jagtap, V.S. Kadam, S.F. Shaikh, M. Ubaidullah, B. Pandit, D.B. Salunkhe, R.S. Patil, *Energy Environ.* **17**, 94–105 (2022)
31. J.S. Lee, K.H. You, C.B. Park, *Adv. Mater.* **24**(8), 1084–1088 (2012)
32. Y.H. Ng, I.V. Lightcap, K. Goodwin, M. Matsumura, P.V. Kamat, *J. Phys. Chem. Lett.* **1**(15), 2222–2227 (2010)
33. B. Li, H. Cao, *J. Mater. Chem.* **21**(10), 3346–3349 (2011)
34. V.V. Gawade, S.R. Sabale, R.S. Dhabbe, S.V. Kite, K.M. Garadkar, *J. Mater. Sci.* **32**, 28573–28586 (2021)

**Publisher's Note** Springer Nature remains neutral with regard to jurisdictional claims in published maps and institutional affiliations.

Springer Nature or its licensor (e.g. a society or other partner) holds exclusive rights to this article under a publishing agreement with the author(s) or other rightsholder(s); author self-archiving of the accepted manuscript version of this article is solely governed by the terms of such publishing agreement and applicable law.